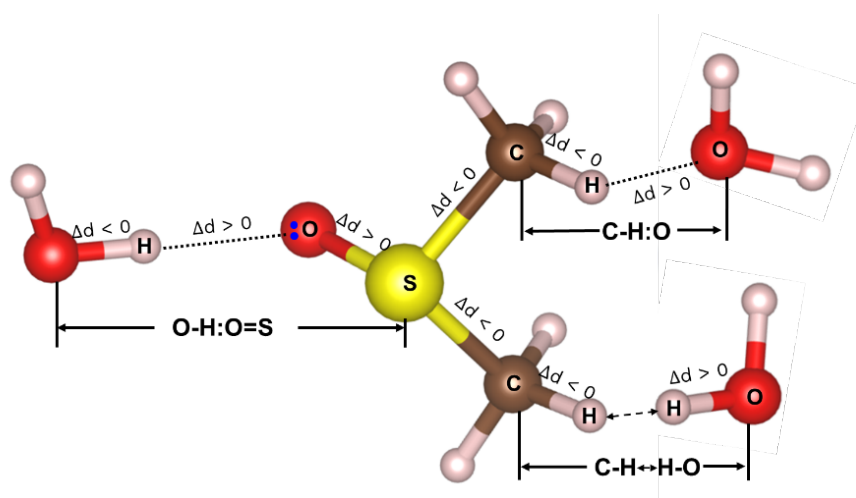


Unprecedented Bonding Dynamics during THF and DMSO Molecular Hydration

Yong Zhou & Chang Q Sun

Research Institute of Interdisciplinary Sciences (RISE) and School of Materials Science & Engineering, Dongguan University of Technology, Dongguan 523808, China

TOC entry



Hydration resolves the O/C-H:O and the charge-inverted H:O-S coupling hydrogen bonds, as well as the H<->H repulsion-engaged C-H<->H-O interactions for DMSO hydration, relaxing discriminatively and cooperatively driven by solute dipolar polarization and coupling interactions.

Abstract

Hydration of organic molecules determines the fascinating properties of aqueous solutions with challenges for understanding the bonding and electronic dynamics. We found three types of unusual interactions in terms of the O/C–H:O coupling hydrogen bonds, the charge-inverted H:O–C and H:O=S, and the H↔H repulsion bridged C–H↔H–O interactions at the THF and DMSO hydration interfaces. Perturbative differential phonon spectroscopy and the first-principles computations further unveiled that the polarization effects of solute dipoles and the inter- and intramolecular coupling interactions cooperatively and disparately relax these bonds. These findings shall enrich the connotation of hydration interfacial bonding profoundly by incorporating the inter- and intramolecular coupling, charge inversion, and the coupling-enabled cooperativity and polarizability upon perturbation, which should offer impacts on dealing with systems involving molecular interactions, such as cryoprotectants, electrolytes, etc.

Keywords: hydration; interface; hydrogen bond; relaxation, driving force.

Understanding how organic molecules interact with water is crucial in fields like health care and medication¹, synthetic chemistry², environmental chemistry³, and renewable energy^{4, 5} etc. The hydration modifies the solvent bonding network and the solution properties. Hydration of small-sized molecules such as methanol, tetrahydrofuran results in the binary aqueous systems performing differently from the pristine water or the organic solutes, such as protein solubility, chemical reactivity, elastoviscosity, surface stress, freezing point, electric and heat conductivity, etc⁶; Hydration of macromolecules, such as deoxyribonucleic acids and proteins, affects the formation of the heterogeneous assemblies and essential biological functions.⁷⁻⁹ As a result, the versatile binary mixtures have found wide-reaching applications serving as cryoprotectants,^{10, 11} cosolvents,¹² clathrates,¹³⁻¹⁵ and electrolytes^{16, 17}, etc. However, little is yet known about the type and dynamical relaxation of the intra-solute and hydration interfacial interactions.

Hydrogen bond (HB) between water and organic molecules plays dominant roles for the properties of a large number of organic solutions. Although the IUPAC has defined the HB ($X^{\delta-}-H^{\delta+}\cdots Y^{\delta-}$) to feature the intermolecular interactions¹⁸ involving the protons and electron lone pairs, the HB is often referred to the $H\cdots Y$ attraction. In the HB, X and Y have a higher electronegativity than H, and therefore X and Y, such as C, N, O, and F, carrying negative charges. The X is referred to as the donor, and the Y as the acceptor of proton H; "-" represents a covalent bond between the X and H, while the "..." represents a nonbond interaction between H and Y. The IUPAC's definition has advanced the properties design and utilization of water and organic crystals which involve the HB.

As a complement to the HB definition from IUPAC, our recent attempt of considering the repulsive force between X—Y in the HB has enabled coupling of the initially isolated intra- and intermolecular interactions (two segments of X—H and $H\cdots Y$, respectively)¹⁹, which amplified the $H\cdots Y$ attraction¹⁸ to the coupling X—H \cdots Y (specifically, O/N/C—H \cdots O) bonds for water and ice¹⁹, aqueous solutions²⁰, and CHNO-based explosives²¹. The coupling O/N/C—H \cdots O bonds relax cooperatively in the bond lengths, energies, and vibration frequencies under a perturbation of pressure, temperature, electric field, and molecular undercoordination¹⁹. For instance, upon external stimulus, both oxygens of the HB of O:H—O travel in the same direction along the HB, but the O:H always relaxes to an extent more than the H—O because of the disparity of these segments ($d_{O:H} \sim 1.6946 \text{ \AA}$, $E_{O:H} \sim 0.1 \text{ eV}$ and $d_{H-O} \sim 1.0004$

Å, $E_{\text{H-O}} \sim 4.0$ eV).

In addition, different from the conventional hydrogen bond, Jabłonski and Civis et al. introduced the concept of charge-inverted hydrogen bond (CIHB, $X^{\delta+}-H^{\delta-}\cdots Y^{\delta+}$) according to their dedicated theoretical and spectroscopic observations.²²⁻²⁵ The CIHB means an interaction between hydrogen atom with partial negative charge and any atom with an electron gap. Furthermore, by extending this CIHB concept, any atom R of lower electronegativity than X and Y can replace the H but ensures the $R\cdots Y$ attraction. However, there is no information about relaxation of the segmental length, energy, and vibration frequency of the CIHB.

To clarify the featured hydration interfacial interactions, we systematically examined the solute polarity and the solute/solvent concentration (number ratio) effect on the relaxation dynamics of the segmented bonds of the THF and DMSO solutes and their hydration interfaces using the combination of the perturbative differential phonon spectroscopy (PDPS)²⁶ and the first-principles computations. THF- and DMSO-water mixtures^{11, 13} play significant roles in unraveling biomolecule hydration and solution molecular behavior. Thus, they are used as representative organic-water systems for investigation. It appears that none of the regular ionic or covalent bonds could form at the hydration interface, but the coupling interactions, such as HBs of $O/C-H\cdots O$, charge-inverted bonds (CIB) of $C/S-O\cdots H$, and $C-H\leftrightarrow H-O$ do exist in the hydration interfaces. The PDPS analysis and computations further unveiled that by increasing the solute/solvent fraction, the polarization induced by the solute dipoles shortens the covalent bonds while elongates the $H\cdots O$ non-bonding of the $O-H\cdots O$, which confirms the essentiality of the $O/C-O$ couplings. The $H\leftrightarrow H$ repulsion lengthens the annexed $O-H$ bond slightly. The $H\cdots O$ attraction and the $S/C-H$ repulsion elongate the $C-O$ and the $S=O$ for the charge-inverted $C-O\cdots H$ in THF and the $S=O\cdots H$ in DMSO. These findings confirm the essentiality of the solute polarization, the charge inversion, and the $O/C-O$ and $S/C-H$ repulsive couplings in dealing with hydration process.

The proposed models of interfacial bonds

To illustrate the possible interfacial bond interactions, we proposed the THF- and DMSO-water

configurations in **Figure 1**. The sp^3 -orbital hybridized carbon has two or three positively-charged hydrogen atoms, and each oxygen has two electron lone pairs marked as ":". Therefore, we also denote the O–H...O as O–H:O in the following discussions. With a relative polarity of 0.207, the THF (C₄H₈O) has eight protons and two pairs of electron lone pairs, compared with the DMSO(C₂H₆SO) of 0.444 polarity having six protons and two electron lone pairs. The distribution of the lone pairs and protons makes the solute dipoles exert an anisotropic electric field to polarize the surrounding water molecules.¹⁹ The H proton and electron lone pair interact with their alike or unlike of the nearby hydrating water molecules to form the possible attractive O:H (conventional hydrogen bond of O/C–H:O and charge-inverted bond of C/S–O:H) and the repulsive H↔H interactions. Neither ionic nor covalent bonds could form at the hydration interface, but bond relaxation and electron polarization occur.

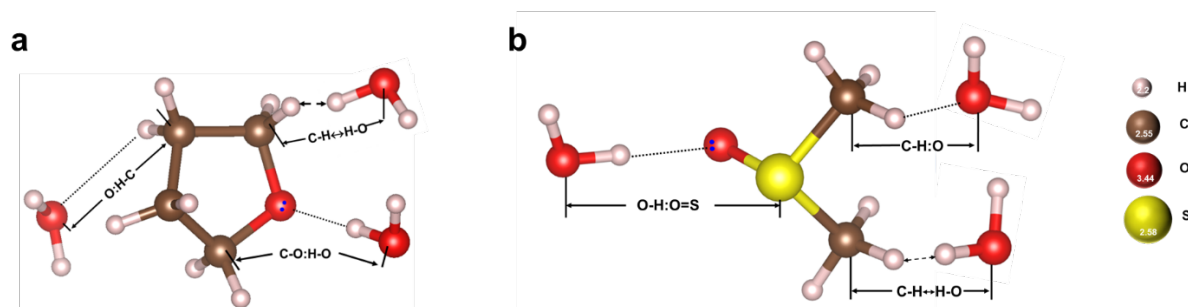


Figure 1. The proposed hydration-interfacial interactions of the (a) THF- and (b) DMSO-water clusters grouped as the HBs of O/C–H...O, CIBs of C/S–O...H interactions, and H↔H repulsion-involved C–H↔H–O. The polarization effect induced by the solute dipoles and the O/C—O or S/C—H repulsive coupling entitle these bonds to relax cooperatively and discriminatively in length and vibration frequency. The electronegativities of the elements are H(2.2), C(2.55), O(3.44), and S(2.58).

Concentration-resolved Raman shift of interfacial bonds upon hydration

Figure 2 shows the solute polarity and concentration resolved Raman spectra of the THF and DMSO solutions. The interfacial H↔H repulsive interactions create no bond as no spectral signature is present. The intensities of the intra-solute C–C/C–O and S–C/S=O bonding vibrations increase as the concentration of organics increases.^{27, 28} To trace the relaxation of the dominate HB in the organic-water mixtures, it would suffice for one to focus on the H–O stretching vibration at 3000–3700 and

the O:H at 50–250 cm^{-1} in the hydration cells.¹⁹

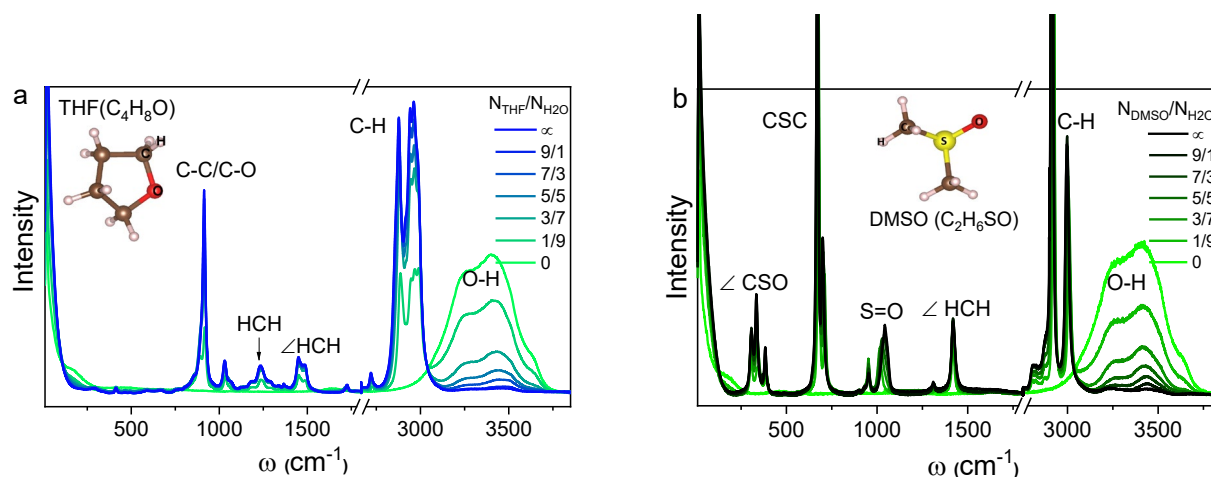


Figure 2. Solute concentration resolved Raman spectra of (a) the THF and (b) the DMSO aqueous solutions with vibrational bonds denoted as oscillations of the specified type of bonds.

However, one can hardly resolve how the individual bond of the hydrating system relaxes upon increasing the solute/solvent concentration from the full-frequency Raman spectra. The PDPS is proven one of the most efficient means for distilling relaxation information of the individual type of bonds in responding to a load of perturbation.^{19, 26, 29} The PDPS proceeds simply by subtracting the referential spectral peak of pristine water from those collected from the concentrated solutions upon all the spectral peaks being normalized. The PDPS peak features the transition of the phonon abundance (peak area), bond stiffness (frequency shift), and structure order (peak width) from the vibration mode of pristine water to the concentrated hydration interfaces. The extent of the segmental frequency shift depends on the relative polarity and the solute/solvent ratio.

In our previous investigation, we have revealed that the electric field shorten and stiffen the H–O bond while the weaker O:H nonbond does the contrast, associated with polarization due to O:H–O bond cooperativity and polarizability¹⁹ (**Figure 3a**). The inhomogeneous charge distribution of a organic molecule is expect to generate a dipole electric field, which exerts the similar polarization effect to the direct-current electric field on the adjacent water molecules (**Figure 3b**).

To examine the above idea, the PDPS refinement was performed. **Figure 3** shows the hydration

interfacial O:H–O bond relaxation where the O:H shifts from 180 to 50 cm^{-1} and the H–O shifts cooperatively from ~ 3160 to ~ 3500 cm^{-1} for both THF and DMSO solutions, which confirms the effect of the solute electric polarization that shortens and stiffens the H–O bond and does the O:H nonbond contrastingly due to the O—O repulsive coupling¹⁹. The frequency shift of the H–O bond from 3160 to 3445 cm^{-1} (Figure 3d) for the DMSO and to 3497 cm^{-1} (Figure 3f) for the THF is reciprocal to the relative polarity of the solute (THF 0.207 vs. DMSO 0.444). The higher polarity of the DMSO polarizes more hydrating H₂O dipoles that screen the DMSO field compared with the THF. Therefore, the stronger inter-DMSO solute repulsion hinders the formation of the hydration cells, as the halide ions do because of their larger ionic volumes²⁰. The narrower O-H peak in PDPS for the DMSO solutions (Figure 3f) than that for the THF (Figure 3d) indicates the higher structure order at the DMSO hydration interface because of its stronger local electric field.

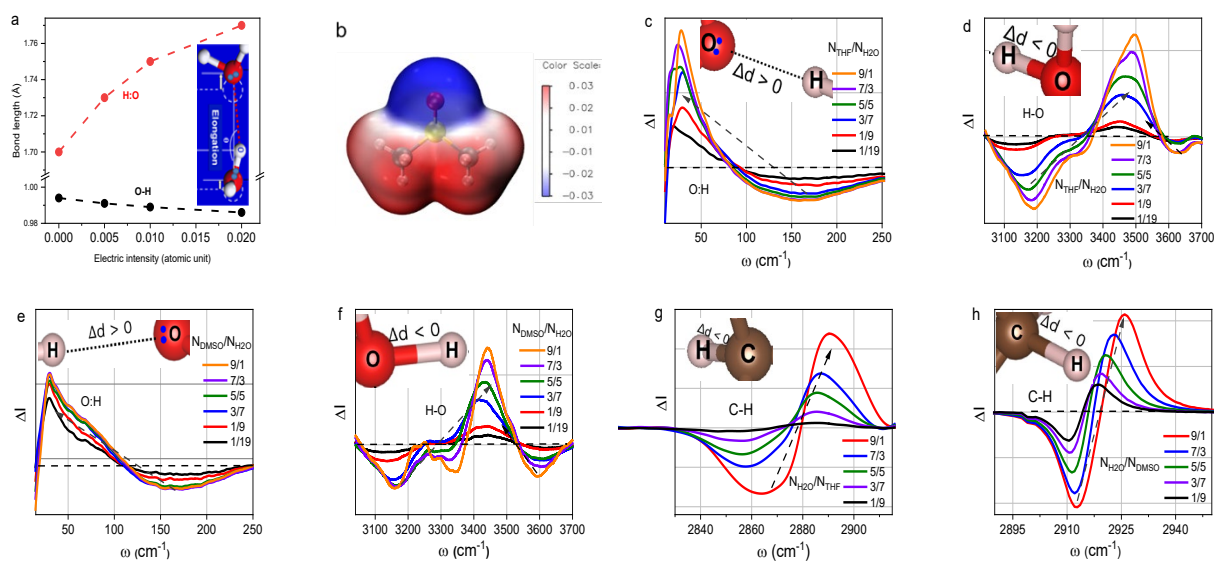


Figure 3. (a) the electric field shorten and stiffen the H–O bond while the weaker O:H nonbond does the contrast, associated with polarization due to O:H–O bond cooperativity and polarizability¹⁹. (b) the electrostatic potential diagram of DMSO molecule, demonstrating a dipole. (c-h) PDPS refinement of the solute type and concentration resolved phonon frequency of (c, e) O:H non-bond, (d, f) H–O bond for the hydration interfacial HB of O:H–O and (g, h) C-H bond blueshift for the HB of C–H:O of THF- and DMSO-water solutions. The 3600 cm^{-1} spectral valley (in d and f) arises from the slight elongation of the polarized shorter H–O bond by the H \leftrightarrow H repulsion .

Upon hydration, the presence of the excess protons breaks the pair-number conservation of protons and electron lone pairs of water, which results in the interfacial C–H \leftrightarrow H–O interactions.¹⁹ The H \leftrightarrow H repulsion has the same effect as mechanic compression³⁰ that lengthens and softens the annexed H–O bond of water and the H–C bond of the solute. As shown in **Figures 3d** and **3f**, the slight red shifting of the $\sim 3600\text{ cm}^{-1}$ band to lower wavenumbers is characteristic of the H \leftrightarrow H repulsion that lengthens the shorter hydrating H–O bond.

The PDPS in **Figure 3g** and **3h** reveals the intra-solute H–C bond stiffening of the O:H–C in THF and DMSO solutions upon increasing the $N_{\text{H}_2\text{O}}/N_{\text{solue}}$ ratio. Increasing the number of H₂O molecules per solute shortens and stiffens the H–C bond. Therefore, the O:H–O and O:H–C follows the same hydrogen bond relaxation regulation¹⁹. This observation also supports the conclusion reached by Scheiner et al.³¹ They have suggested that the C–H \cdots O (equal to O:H–C in our discussion) interaction exhibits similarities to the conventional O–H \cdots O (equal to O:H–O in our discussion) in terms of shifts in electron density, magnitudes of interaction energy components, and equilibrium geometry preference on the basis of ab initio calculations with a focus on the interaction between F_nH_{3–n}CH (proton donor) and H₂O, CH₃OH, and H₂CO (acceptors). Therefore, the hydrogen bond nature of O:H–C would make it behave like to other hydrogen bond, regardless of their strength.

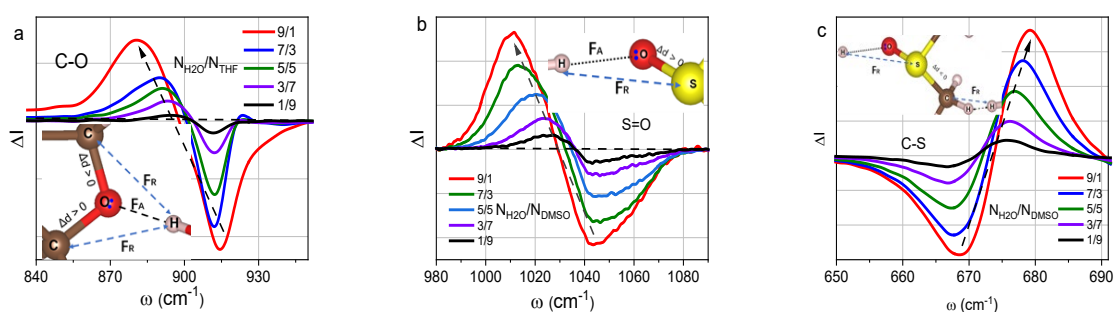


Figure 4. PDPS refinement of the solute type and $N_{\text{H}_2\text{O}}/N_{\text{solue}}$ concentration resolved the redshifts of C–O and S=O phonon frequency for the (a) H:O–C in the THF and for the (d) H:O=S in the DMSO, and C–S phonon frequency blueshift in the DMSO. Insets display the schematic illustration of the corresponding force diagram for the CIBs in THF and DMSO and F_A and F_R represent attraction and repulsive force between the atoms, respectively.

In contrast, the C–O and S=O bonds in the charge-inverted bonds of C–O:H and S=O:H relax contrastingly to the intra-solute C–H as the $N_{\text{H}_2\text{O}}$ increases per solute molecule. We can analyze the forces acting on the C–O:H and S=O:H that are subject to the combination of the O:H attraction and the C/S—H repulsion, which lengthens the C–O and S=O as the $N_{\text{H}_2\text{O}}$ per solute increases (**Figure 4a** and **4b**). The vibration frequency of the intra-solute C–C bond of $\sim 910\text{ cm}^{-1}$ overlaps that of the C–O, so one can hardly distinguish the C–C frequency shift during hydration.

The softening of the intra-solute C–O and S=O bond in the charge-inverted bonds of C–O:H and S=O:H with increasing the $N_{\text{H}_2\text{O}}$ per solute resembles that observed from the $\text{Me}_3\text{Si}^{\delta+}-\text{H}^{\delta-}\cdots\text{Y}^{\delta+}$ complexes ($\text{Y} = \text{ICF}_3, \text{BrCN}, \text{HCN}$) using low-temperature IR.²⁵ The consistency of the IR and the PDPS observations evidences the softening of Si–H, C–O and S=O in the charge-inverted bonds arises from the combination of the H:O nonbond attraction and the C/S—H repulsive coupling.

In addition, the C–S stretching in DMSO undergoes blueshift upon increasing the $N_{\text{H}_2\text{O}}$ per solute molecule, see **Figure 4c**. The interplay of the S—H repulsion and the C–H \leftrightarrow H–O repulsion shortens the C–S bond upon hydration.

DFT quantification of the bond length variations upon hydration

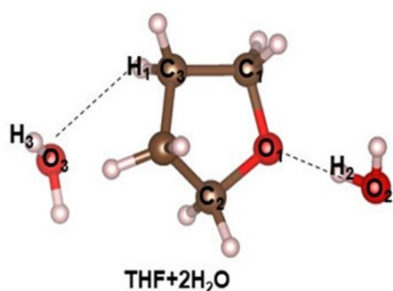
To quantify the bond length change of interfacial bonds, which requires the explicit presence of water, and we assuming the electrostatic interaction between the solvent and the solute need to be described by the implicit solvent model. That motives we used the hybrid solvation models. Such hybrid explicit/continuum solvation models are often used in the cases where first solvation shell is considered.³²⁻³⁴ Different from the proposed organic-water clusters involving three H_2O molecules, the structural configurations for DFT-D3 computing bond relaxation upon the THF and DMSO being hydrated by $2\text{H}_2\text{O}$ molecules adapt to the Polarizable Continuum model. They were fully optimized associated with frequency calculations to ensure they are minimum on the potential surface.

As listed in **Table 1** and **Table 2**, the simulation outcomes agree with the measured phonon frequency shifts. The relaxation of the bond length and energy in terms of vibration frequency that features the

stiffness of an oscillating dimer in responding to a load of perturbation. One can readily correlate the frequency shift ($\Delta\omega$) to the relaxation of bond length (d) through the equation of frequency shift (we have described it in the section of **Method**), which suggests that if a phonon peak undergoes redshift, its vibrating bond will expand and both the bond energy (E) and the bond length relax in opposite directions. Specifically, the THF hydration shortens the H–O bond by -2.04 % and lengthens the H:O by 6.04%. DMSO hydration displays a similar bond length variation, showing -1.64% and 3.74% strain for the H–O and the H:O, respectively. Regarding to the intra-solute bonds, the C–O of THF and S=O bonds of DMSO become longer indeed compared with those in the pure organic molecules. The O:H strain for the O:H–C is much greater than that for the O:H–O (6.04% vs.65.23% for THF and 3.74% vs.44.69% for DMSO) due to the hydrophobicity effect of the methyl functionalities.³⁵ The C-S contract -0.38% compared to those in its parent DMSO.


Table 1. Bond length relaxation of the THF+2H₂O with respect to that of the pristine water and organics.

THF (Ref.)		THF+2H ₂ O (solution)		
Bond	$d(\text{\AA})$	Bond	$d(\text{\AA})$	Strain (%)
O ₁ -C ₁	1.444	O ₁ -C ₁	1.454	0.69%
O ₁ -C ₂	1.444	O ₁ -C ₂	1.447	0.21%
C ₃ -H ₁	1.093	O ₁ :H ₂	1.797	6.04%
		O ₂ -H ₂	0.980	-2.04%
		C ₃ -H ₁	1.091	-0.18%
		O ₃ :H ₁	2.800	65.23%
		O ₃ -H ₃	0.964	-3.64%



*The bond lengths of O:H and H-O for the reference H₂O are 1.6946 Å and 1.004 Å, respectively.¹⁹

Table 2. Bond length relaxation of the DMSO+2H₂O with respect to that of the pristine water and organics.

DMSO		DMSO+2H ₂ O (solution)		
Bond	<i>d</i> (Å)	Bond	<i>d</i> (Å)	Strain (%)
O ₁ =S	1.544	O ₂ -H ₂	0.984	-1.64%
C-H ₁	1.090	O ₁ :H ₂	1.758	3.74%
S-C	1.833	O ₁ =S	1.557	0.84%
 <p>DMSO+2H₂O</p>		C-H ₁	0.965	-11.47%
		O ₃ :H ₁	2.452	44.69%
		H ₃ -O ₃	0.965	-3.54%
		S-C	1.826	-0.38%

*The bond lengths of O:H and H-O for the reference H₂O are 1.6946 Å and 1.004 Å, respectively.¹⁹

Conclusion

In this work, to explore the bond type and relaxation dynamics at the hydration interfacial, the relative polarity and concentration effects on the vibrational frequencies and bond length of THF- and DMSO-water binary solution were investigated. Using the combined techniques of the PDPS analysis and DFT computation, we have clarified that:

- i. Three unusual types of molecular interactions. Those are: 1) the coupling O–H:O and C–H:O bonds, 2) the charge-inverted H:O-C and H:O=S, and 3) the H↔H repulsion bridged C-H↔H-O interactions at the THF and DMSO hydration interfaces.
- ii. Forces driving the disparate and cooperative relaxation of the bonding segments. The polarization effect induced by the solute dipoles and the inter- and intramolecular coupling interactions cooperatively and disparately relax the bonds of both the solutes and the hydration interfaces.

These findings would enrich the connotation of hydration interfacial bonding profoundly by incorporating the coupling, charge inversion, and coupling-enabled cooperativity and polarizability upon perturbation, which should offer alternative impacts on dealing with systems involving molecular interactions, such as cryoprotectants, electrolytes, etc.

Methods

Materials

Organic reagents of tetrahydrofuran (THF, 99.9%) and dimethyl sulfoxide (DMSO, 99.7%) were purchased from Shanghai Titan Scientific Co., Ltd. All chemicals were of analytical grade and used without further purification. Deionized water was used as a solvent throughout the experiments.

Raman measurements

Raman spectra measurements were carried out on a confocal Raman spectrometer (HORIBA) in a back-scattering configuration with a spectral resolution of 1 cm^{-1} . 150 μL of deionized water or binary organic-aqueous solution was injected into a customized quartz cell and excited by a laser (emission wavelength of 532 nm, output power 50 mW) at room temperature. A 10 \times long-working-distance objective was used to focus laser light onto the sample and collect the scattered light. The signal was detected by a multichannel ultra-low temperature (213 K) charge-coupled array detector. The Raman spectra in the wavenumber range of 10–4000 cm^{-1} were recorded. Each spectrum is an accumulation of a single scan with an exposure time of 10 s.

The perturbative differential phonon spectroscopy (PDPS) analysis method

A perturbative Raman spectroscopy refines the relaxation of the bond length and energy in terms of vibration frequency ω that features the stiffness of a oscillating dimer in responding to a load of perturbation. The vibration frequency corresponds to the curvature of the potential at equilibrium, $u(r)$. From the perspective of dimensionality, the $\Delta\omega$ shift depends on the division of the square root of the bond energy E by the bond length d with μ being the reduced mass of the vibrating dimer. The

following equations describe the perturbative differential phonon spectroscopic (PDPS) method:³⁶

$$\left\{ \begin{array}{l} \Delta\omega = \sqrt{\frac{\partial^2 u(r)}{\mu \partial r^2}} \Big|_{r=d} \propto \sqrt{\frac{E}{\mu d^2}} \quad \text{(a: frequency shift)} \\ \frac{d\text{Ln}(\omega)}{d\text{Ln}(r)} = -\left(1 + \frac{r_0}{2E_0} \left| \frac{dE}{dr} \right| \right) \quad \text{(b: extended Gruneisen)} \\ \Delta I_{DPS}(\omega) = \frac{I_q(\omega)}{\int_{\omega_n}^{\omega_M} I_q(\omega) d\omega} - \frac{I_{ref}(\omega)}{\int_{\omega_n}^{\omega_M} I_{ref}(\omega) d\omega} \quad \text{(c: DPS refinement intensity)} \end{array} \right.$$

One can readily correlate the frequency shift ($\Delta\omega$) to the relaxation of bond length (d) through the equation of frequency shift, which suggests that if a phonon peak undergoes redshift, its vibrating bond will expand and both the bond energy (E) and the d relax in opposite directions.

The $-dE/dr$ is the force $F(x_0+\delta(q))$ of the relaxed dimer upon $\delta(q)$ amount of relaxation under the q perturbation. The q is an applied field such as compression, temperature, or electrification used as a probe during detection. During the PDPS analysis, the spectra are collected under identical conditions. After background correction and peak area normalization for all the spectra, we could derive the valuable PDPS information by subtracting the referential spectrum (here the pure water or organics) from the concerned samples. The resulting PDPS provides crucial indications of the contraction or elongation of corresponding bond by evaluating the $\Delta\omega$. In the PDPS, the regions above and below the lateral axis correspondingly represent the net gain and loss of phonon abundance. The peak integral refines the abundance transition of the frequency $\Delta\omega$ and structural order of concerned samples. In the present Raman investigations, to eliminate the possible effect of the $-CH$ stretching vibration on the $-OH$ stretching vibration, the Raman spectrum in the range of $3050\text{-}3850\text{cm}^{-1}$ was selected for H—O analysis and the baseline was subtracted from the data using the exponential function.

Computational method and models

The restricted B3LYP exchange-correlation functional was used for all calculations with the Gaussian 09 program³⁷ suite employing the TZVP³⁸ basis set. The DFT-D3 method³⁹ was consistently

used to include the dispersion contribution. Solvation effects were considered implicitly using the Polarizable Continuum Model (PCM) model.

Declaration of competing interest

No competing financial interests or personal relationships are declared.

Acknowledgments

Financial supports received from the National Natural Science Foundation of China (12304243; 11832019) and Guangdong Provincial Key Laboratory of Extreme Conditions (2023B1212010002) are gratefully acknowledged.

References

1. Serdakowski, A. L.; Dordick, J. S., Enzyme activation for organic solvents made easy. *Trends in Biotechnology* **2008**, *26* (1), 48-54.
2. Zhou, Y.; Kadam, S. A.; Shamzhy, M.; Cejka, J.; Opanasenko, M., Isorecticular UTL-derived zeolites as model materials for probing pore size–activity relationship. *ACS Catalysis* **2019**, *9* (6), 5136-5146.
3. Dong, C.; Marinova, M.; Tayeb, K. B.; Safonova, O. V.; Zhou, Y.; Hu, D.; Chernyak, S.; Corda, M.; Zaffran, J.; Khodakov, A. Y., Direct photocatalytic synthesis of acetic acid from methane and CO at ambient temperature using water as oxidant. *Journal of the American Chemical Society* **2023**, *145* (2), 1185-1193.
4. Han, D.; Cui, C.; Zhang, K.; Wang, Z.; Gao, J.; Guo, Y.; Zhang, Z.; Wu, S.; Yin, L.; Weng, Z., A non-flammable hydrous organic electrolyte for sustainable zinc batteries. *Nature Sustainability* **2022**, *5* (3), 205-213.
5. Han, M.; Huang, J.; Xie, X.; Li, T. C.; Huang, J.; Liang, S.; Zhou, J.; Fan, H. J., Hydrated eutectic electrolyte with ligand-oriented solvation shell to boost the stability of zinc battery. *Advanced Functional Materials* **2022**, *32* (25), 2110957.
6. Andreev, M.; de Pablo, J. J.; Chremos, A.; Douglas, J. F., Influence of ion solvation on the properties of electrolyte solutions. *The Journal of Physical Chemistry B* **2018**, *122* (14), 4029-4034.
7. Chremos, A.; Douglas, J. F., Polyelectrolyte association and solvation. *The Journal of Chemical Physics* **2018**, *149* (16), 163305.
8. Liu, L.; Besenbacher, F.; Dong, M., Self-assembly of DNA bases via hydrogen bonding studied by scanning tunneling microscopy. In *Nucleic Acid Nanotechnology*, Springer: 2013; pp 3-21.
9. Zhao, H.; Song, X.; Aslan, H.; Liu, B.; Wang, J.; Wang, L.; Besenbacher, F.; Dong, M., Self-assembly of hydrogen-bonded supramolecular complexes of nucleic-acid-base and fatty-acid at the liquid–solid interface. *Physical Chemistry Chemical Physics* **2016**, *18* (21), 14168-14171.
10. Li, D.-X.; Liu, B.-L.; Liu, Y.-s.; Chen, C.-l., Predict the glass transition temperature of glycerol–water binary cryoprotectant by molecular dynamic simulation. *Cryobiology* **2008**, *56* (2), 114-119.
11. Notman, R.; Noro, M.; O'Malley, B.; Anwar, J., Molecular basis for dimethylsulfoxide (DMSO) action on lipid

- membranes. *Journal of the American Chemical Society* **2006**, *128* (43), 13982-13983.
12. Smith, M. D.; Mostofian, B.; Cheng, X.; Petridis, L.; Cai, C. M.; Wyman, C. E.; Smith, J. C., Cosolvent pretreatment in cellulosic biofuel production: effect of tetrahydrofuran-water on lignin structure and dynamics. *Green Chemistry* **2016**, *18* (5), 1268-1277.
 13. Anderson, R.; Chapoy, A.; Tohidi, B., Phase relations and binary clathrate hydrate formation in the system H₂-THF- H₂O. *Langmuir* **2007**, *23* (6), 3440-3444.
 14. Kim, D.-Y.; Park, J.; Lee, J.-w.; Ripmeester, J. A.; Lee, H., Critical guest concentration and complete tuning pattern appearing in the binary clathrate hydrates. *Journal of the American Chemical Society* **2006**, *128* (48), 15360-15361.
 15. Shin, H. J.; Lee, Y.-J.; Im, J.-H.; Han, K. W.; Lee, J.-W.; Lee, Y.; Lee, J. D.; Jang, W.-Y.; Yoon, J.-H., Thermodynamic stability, spectroscopic identification and cage occupation of binary CO₂ clathrate hydrates. *Chemical Engineering Science* **2009**, *64* (24), 5125-5130.
 16. Huang, J.; Dong, X.; Guo, Z.; Wang, Y., Progress of organic electrodes in aqueous electrolyte for energy storage and conversion. *Angewandte Chemie* **2020**, *132* (42), 18478-18489.
 17. Xiao, D.; Dou, Q.; Zhang, L.; Ma, Y.; Shi, S.; Lei, S.; Yu, H.; Yan, X., Optimization of organic/water hybrid electrolytes for high-rate carbon-based supercapacitor. *Advanced Functional Materials* **2019**, *29* (42), 1904136.
 18. Arunan, E.; Desiraju, G. R.; Klein, R. A.; Sadlej, J.; Scheiner, S.; Alkorta, I.; Clary, D. C.; Crabtree, R. H.; Dannenberg, J. J.; Hobza, P., Defining the hydrogen bond: An account (IUPAC Technical Report). *Pure and Applied Chemistry* **2011**, *83* (8), 1619-1636.
 19. Sun, C. Q.; Huang, Y.; Zhang, X.; Ma, Z.; Wang, B., The physics behind water irregularity. *Physics Reports* **2023**, *998*, 1-68.
 20. Sun, C. Q., Aqueous charge injection: solvation bonding dynamics, molecular nonbond interactions, and extraordinary solute capabilities. *International Reviews in Physical Chemistry* **2018**, *37* (3-4), 363-558.
 21. Wang, J.; Zeng, Y.; Zheng, Z.; Zhang, L.; Wang, B.; Yang, Y.; Sun, C. Q., Discriminative Mechanical and Thermal Response of the H-N Bonds for the Energetic LLM-105 Molecular Assembly. *The Journal of Physical Chemistry Letters* **2023**, *14* (38), 8555-8562.
 22. Jabłoński, M., Red and blue shifted hydridic bonds. *Journal of Computational Chemistry* **2014**, *35* (24), 1739-1747.
 23. Jabłoński, M., Theoretical insight into the nature of the intermolecular charge-inverted hydrogen bond. *Computational and Theoretical Chemistry* **2012**, *998*, 39-45.
 24. Jabłoński, M., Binding of X-H to the lone-pair vacancy: Charge-inverted hydrogen bond. *Chemical Physics Letters* **2009**, *477* (4-6), 374-376.
 25. Civis, S.; Lamanec, M.; Špirko, V. r.; Kubista, J.; Špet'ko, M.; Hobza, P., Hydrogen Bonding with Hydridic Hydrogen-Experimental Low-Temperature IR and Computational Study: Is a Revised Definition of Hydrogen Bonding Appropriate? *Journal of the American Chemical Society* **2023**, *145* (15), 8550-8559.
 26. Liu, X. J.; Zhang, X.; Bo, M. L.; Li, L.; Nie, Y. G.; Tian, H.; Sun, Y.; Xu, S.; Wang, Y.; Zheng, W.; Sun, C. Q., Coordination-resolved electron spectrometrics. *Chemical Reviews* **2015**, *115* (14), 6746-6810.
 27. Raj, A.; Chen, Y. J.; Wang, C. L.; Hamaguchi, H. o., Raman spectra and structure of hydrogen-bonded water oligomers in tetrahydrofuran-H₂O binary solutions. *Journal of Raman Spectroscopy* **2022**, *53* (10), 1710-1721.
 28. Ojha, A. K.; Srivastava, S. K.; Peica, N.; Schlücker, S.; Kiefer, W.; Asthana, B. P., Concentration dependent wavenumber shifts and linewidth changes of some prominent vibrational modes of C₄H₈O investigated in a binary system (C₄H₈O+H₂O) by polarized Raman study and ab initio calculations. *Journal of Molecular Structure* **2005**, *735-736*, 349-357.
 29. Zhou, Y.; Li, L.; Huang, Y.; Ou, J.; Li, W.; Sun, C. Q., Perturbative vibration of the coupled hydrogen-bond (O-H-O) in water. *Advances in Colloid and Interface Science* **2022**, *310*, 102809.

30. Zhou, Y.; Gong, Y.; Huang, Y.; Ma, Z.; Zhang, X.; Sun, C. Q., Fraction and stiffness transition from the HO vibrational mode of ordinary water to the HI, NaI, and NaOH hydration states. *Journal of Molecular Liquids* **2017**, *244*, 415-421.
31. Gu, Y.; Kar, T.; Scheiner, S., Fundamental properties of the CH \cdots O interaction: is it a true hydrogen bond? *Journal of the American Chemical Society* **1999**, *121* (40), 9411-9422.
32. Xin, X.; Niu, X.; Liu, W.; Wang, D., Hybrid Solvation Model with First Solvation Shell for Calculation of Solvation Free Energy. *ChemPhysChem* **2020**, *21* (8), 762-769.
33. Porto, C. M.; Santana, L. C.; Morgon, N. H., Theoretical investigation of the cooperative effect of solvent: a case study. *Physical Chemistry Chemical Physics* **2022**, *24* (23), 14603-14615.
34. Dague, Y.; Koyambo-Konzapa, S.-J.; Nose, H.; Minguirbara, A.; Nsangou, M.; Amolo, G., DFT investigation on the structural and vibrational behaviours of the non-protein amino acids in hybrid explicit/continuum solvent: a case of the zwitterions γ -aminobutyric and α -aminoisobutyric acids. *Journal of Molecular Modeling* **2024**, *30* (1), 17.
35. Murshid, N.; Wang, X., Hydrophobic effect of alkyl groups stabilizing self-assembled colloids in water. *The Journal of Physical Chemistry B* **2017**, *121* (25), 6280-6285.
36. Liu, X. J.; Bo, M. L.; Zhang, X.; Li, L.; Nie, Y. G.; Tian, H.; Sun, Y.; Xu, S.; Wang, Y.; Zheng, W.; Sun, C. Q., Coordination-resolved electron spectrometrics. *Chemical Reviews* **2015**, *115* (14), 6746-6810.
37. Frisch, M. J. T., G. W.; Schlegel, H. B.; Scuseria, G. E.; Robb, M. A.; Cheeseman, J. R.; Scalmani, G.; Barone, V.; Petersson, G. A.; Nakatsuji, H.; Li, X.; Caricato, M.; Marenich, A. V.; Bloino, J.; Janesko, B. G.; Gomperts, R.; Mennucci, B.; Hratchian, H. P.; Ortiz, J. V.; Izmaylov, A. F.; Sonnenberg, J. L.; Williams, Ding, F.; Lipparini, F.; Egidi, F.; Goings, J.; Peng, B.; Petrone, A.; Henderson, T.; Ranasinghe, D.; Zakrzewski, V. G.; Gao, J.; Rega, N.; Zheng, G.; Liang, W.; Hada, M.; Ehara, M.; Toyota, K.; Fukuda, R.; Hasegawa, J.; Ishida, M.; Nakajima, T.; Honda, Y.; Kitao, O.; Nakai, H.; Vreven, T.; Throssell, K.; Montgomery Jr., J. A.; Peralta, J. E.; Ogliaro, F.; Bearpark, M. J.; Heyd, J. J.; Brothers, E. N.; Kudin, K. N.; Staroverov, V. N.; Keith, T. A.; Kobayashi, R.; Normand, J.; Raghavachari, K.; Rendell, A. P.; Burant, J. C.; Iyengar, S. S.; Tomasi, J.; Cossi, M.; Millam, J. M.; Klene, M.; Adamo, C.; Cammi, R.; Ochterski, J. W.; Martin, R. L.; Morokuma, K.; Farkas, O.; Foresman, J. B.; Fox, D. J., Gaussian 09 Rev. D01. Gaussian, Inc.: Wallingford, CT, 2016.
38. Schäfer, A.; Huber, C.; Ahlrichs, R., Fully optimized contracted Gaussian basis sets of triple zeta valence quality for atoms Li to Kr. *The Journal of Chemical Physics* **1994**, *100* (8), 5829-5835.
39. Grimme, S.; Antony, J.; Ehrlich, S.; Krieg, H., A consistent and accurate ab initio parametrization of density functional dispersion correction (DFT-D) for the 94 elements H-Pu. *The Journal of Chemical Physics* **2010**, *132* (15).